

Article

Sensorless Direct Torque Control of Surface-Mounted Permanent Magnet Synchronous Motors with Nonlinear Kalman Filtering

Joon B. Park [†] and Xin Wang ^{*,†} 

Electrical and Computer Engineering, Southern Illinois University, Edwardsville, IL 62026, USA; joopark@siue.edu

* Correspondence: xwang@siue.edu; Tel.: +1-618-650-3634

† These authors contributed equally to this work.

Received: 2 April 2018; Accepted: 16 April 2018; Published: 18 April 2018



Abstract: The demand for sensorless control of surface-mounted permanent magnet synchronous motor drives has grown rapidly. Among various sensorless control techniques developed, Matsui's current model-based approach and the extended Kalman filter approach have gained much attention. However, the performance of these control methods can be severely worsened or may even become unstable under strong disturbances or sensing failures. This paper presents a comparative study of the extended Kalman filter, the resilient extended Kalman filter, and the unscented Kalman filter-based sensorless direct torque and flux control approaches for the surface-mounted permanent magnet synchronous motor drives. Computer simulation studies and hardware implementation results have shown the efficiency and superior performance of the resilient extended Kalman filter and the unscented Kalman filter over the traditional extended Kalman filter for sensorless direct torque control applications.

Keywords: permanent magnet synchronous motors; Kalman filtering; sensorless control

1. Introduction

Over the past decades, there has been a rapid increase in the deployment of surface-mounted permanent magnet synchronous motors (SPMSM) in industrial and commercial applications, such as wind energy conversion systems, hybrid electric vehicles, robotics, home appliances, etc. Adjustable speed SPM drives offer many distinct advantages including large torque to weight ratio, wide constant-power operating range, high efficiency and reliability, etc.

A wide variety of adjustable-speed control techniques have been studied in literature for permanent magnet AC motors. Among them, field oriented control (FOC) for SPMSM drives has reached industrial application maturity. FOC requires coordinate transforms and space-vector pulse width modulation (SVPWM), through which the flux and torque of AC machines are controlled independently [1–5]. In order to eliminate these requirements, direct torque control (DTC) was proposed as a powerful alternative [6,7]. The advantages of DTC include fast dynamic responses, elimination of coordinate transforms and SVPWM. DTC also has minor disadvantages, in comparison with FOC, including: difficulties to control torque and flux at relatively low speed, variable switching frequency, larger harmonics, larger noise level and ripples at low speed range. Despite the aforementioned shortcomings, DTC is also a feasible solution for commercial permanent magnet AC drives.

DTC is in nature “sensorless”, as rotor position is not required for performing coordinate transform [6,7]. However, it relies on the information of stator flux vector. Especially, at relatively

low speed range, due to inaccurate estimation of flux vector, DTC suffers from the performance degradation. Sensorless estimation of stator flux and rotor speed has to be designed to preserve the advantages of direct torque control. For traditional DTC, stator flux linkage (λ_s) is estimated through integrating stator induced voltage over time.

$$\lambda_s(t) = \int (v_s - R_s i_s) dt + \lambda_s(0) \quad (1)$$

Even minor dc offsets in voltage or current signals accumulated by integration will form a substantial disturbance. Hence, traditional estimation of λ_s contains large and noisy ripples [8–10].

To improve the estimation of stator flux linkage, various estimators have been developed including the back-emf integration methods such as low-pass filtering [11–13], and stabilizing the integrator with a PI-corrector or current offset methods [14–17]. However, these approaches are not designed for real-time estimation. The sliding mode observer (SMO) is developed for providing real-time state estimates for permanent magnet synchronous motors in [18–20]. However, higher-order derivatives presented in SMO are not desirable for hardware implementations. The extended Kalman filter (EKF) is a popular approach for sensorless control scheme. However, the performance of EKF deteriorates or may even become unstable under measurement failure conditions [21–27].

To improve EKF performance under external disturbances, noise and measurement failures, this paper presents a comparative study of the extended Kalman filter (EKF), the resilient extended Kalman filter (REKF), and the unscented Kalman filter (UKF)-based sensorless direct torque control approaches for SPMSM drives. Computer simulation studies and hardware implementation results have shown the efficiency and superior performance of the resilient extended Kalman filter and the unscented Kalman filter over the traditional extended Kalman filter for sensorless direct torque control applications.

This paper is organized as follows: Section 2 presents the dynamics of surface-mounted permanent magnet synchronous motors. Section 3 provides the overall control scheme of direct torque control. Section 4 presents the traditional extended Kalman filtering, the resilient extended Kalman filter and the unscented Kalman filter for nonlinear estimation. Computer simulation results and hardware implementation results are illustrated in Section 5. Finally, conclusions are summarized in Section 6.

2. Dynamics of Surface-Mounted Permanent Magnet Synchronous Motors

Applying Park's transform, the surface-mounted permanent magnet synchronous motors (SPMSM) can be modeled as follows:

$$v_d = R_s i_d + \frac{d\lambda_d}{dt} - \omega_e \lambda_q \quad (2)$$

$$v_q = R_s i_q + \frac{d\lambda_q}{dt} + \omega_e \lambda_d \quad (3)$$

$$\lambda_d = L_s i_d + \lambda_m \quad (4)$$

$$\lambda_q = L_s i_q \quad (5)$$

It should be noted that the direct and quadrature axis stator inductance are the same for SPMSM, i.e., $L_d = L_q = L_s$, as no rotor saliency exists.

Equivalently, the current frame of reference model can be reached as follows:

$$\frac{di_d}{dt} = -\frac{R_s}{L_s} i_d + \omega_e i_q + \frac{1}{L_s} v_d \quad (6)$$

$$\frac{di_q}{dt} = -\frac{R_s}{L_s} i_q - \omega_e i_d - \omega_e \frac{\lambda_m}{L_s} + \frac{1}{L_s} v_q \quad (7)$$

The developed electromechanical torque is

$$\tau_e = \frac{3}{2} \frac{P}{2} \lambda_m i_q \quad (8)$$

Note that the mechanical and electrical angular velocities are related by

$$\omega_e = \frac{P}{2} \omega_m \quad (9)$$

The mechanical dynamics can be summarized as

$$\frac{d\omega_m}{dt} = \frac{1}{J} (\tau_e - \tau_l - D\omega_m) \quad (10)$$

Applying (8) and (9), we have

$$\frac{d\omega_e}{dt} = \frac{3}{2J} \left(\frac{P}{2}\right)^2 \lambda_m i_q - \frac{P}{2J} \tau_l - \frac{D}{J} \omega_e, \quad (11)$$

and

$$\frac{d\theta_e}{dt} = \omega_e \quad (12)$$

The external torque load τ_l is also considered as state variable, which is assumed to be constant over a brief period of sampling time T_s , i.e., we have

$$\frac{d\tau_l}{dt} \approx 0 \quad (13)$$

The continuous-time SPMSM state space model can be written as follows:

$$\dot{x} = \frac{d}{dt} \begin{bmatrix} i_d \\ i_q \\ \omega_e \\ \theta_e \\ \tau_l \end{bmatrix}; x = \begin{bmatrix} i_d \\ i_q \\ \omega_e \\ \theta_e \\ \tau_l \end{bmatrix}; u = \begin{bmatrix} v_d \\ v_q \end{bmatrix}; y = \begin{bmatrix} i_d \\ i_q \end{bmatrix} \quad (14)$$

$$\dot{x} = A_c(x) + B_c(u) = f(x, u) \quad (15)$$

$$y = h_c(x) = h(x, u), \quad (16)$$

where we have

$$A_c = \begin{bmatrix} -\frac{R_s}{L_s} & \omega_e & 0 & 0 & 0 \\ -\omega_e & -\frac{R_s}{L_s} & -\frac{\lambda_m}{L_s} & 0 & 0 \\ 0 & \beta \lambda_m & -\frac{D}{J} & 0 & -\frac{P}{2J} \\ 0 & 0 & 1 & 0 & 0 \\ 0 & 0 & 0 & 0 & 0 \end{bmatrix}; B_c = \begin{bmatrix} \frac{1}{L_s} & 0 \\ 0 & \frac{1}{L_s} \\ 0 & 0 \\ 0 & 0 \\ 0 & 0 \end{bmatrix}; h_c = \begin{bmatrix} 1 & 0 & 0 & 0 & 0 \\ 0 & 1 & 0 & 0 & 0 \end{bmatrix} \quad (17)$$

and

$$\beta = \frac{3}{2J} \left(\frac{P}{2}\right)^2 \quad (18)$$

Notice that subscript c represents continuous-time signals.

Applying Euler's discretization, the discrete-time system model can be reached as follows:

$$\begin{aligned}x_{k+1} &= x_k + T_s f(x_k, u_k) \\ y_k &= h(x_k, u_k)\end{aligned}\quad (19)$$

where T_s is the sampling time.

Based on Jacobian matrices computation, a linear-time-invariant discrete-time state space model can be reached as follows:

$$\hat{x}_{k+1} = \begin{bmatrix} i_d(\hat{x}_{k+1}) \\ i_q(\hat{x}_{k+1}) \\ \omega_e(\hat{x}_{k+1}) \\ \theta_e(\hat{x}_{k+1}) \\ \tau_l(\hat{x}_{k+1}) \end{bmatrix} = A_k \begin{bmatrix} i_d(\hat{x}_k) \\ i_q(\hat{x}_k) \\ \omega_e(\hat{x}_k) \\ \theta_e(\hat{x}_k) \\ \tau_l(\hat{x}_k) \end{bmatrix} + B_k \begin{bmatrix} v_d(\hat{x}_k) \\ v_q(\hat{x}_k) \end{bmatrix}, \quad (20)$$

where we have

$$A_k = I + \left. \frac{\partial f(x_k, u_k)}{\partial x} \right|_{x=\hat{x}_k} \cdot T_s = \begin{bmatrix} 1 - \frac{R_s}{L_s} T_s & \omega_e T_s & i_q T_s & 0 & 0 \\ -\omega_e T_s & 1 - \frac{R_s}{L_s} T_s & -(i_d + \frac{\lambda_m}{L_s}) T_s & 0 & 0 \\ 0 & \beta \lambda_m T_s & 1 - \frac{D}{J} T_s & 0 & -\frac{P}{2J} T_s \\ 0 & 0 & T_s & 1 & 0 \\ 0 & 0 & 0 & 0 & 1 \end{bmatrix} \quad (21)$$

Similarly,

$$B_k = \left. \frac{\partial f(x_k, u_k)}{\partial u} \right|_{x=\hat{x}_k} \cdot T_s = \begin{bmatrix} \frac{T_s}{L_s} & 0 \\ 0 & \frac{T_s}{L_s} \\ 0 & 0 \\ 0 & 0 \\ 0 & 0 \end{bmatrix} \quad (22)$$

The measurement equation can be expressed as:

$$y_k = h_k(x_k) = \begin{bmatrix} i_d \\ i_q \end{bmatrix} = C_k \begin{bmatrix} i_d \\ i_q \\ \omega_e \\ \theta_e \\ \tau_l \end{bmatrix}, \quad (23)$$

and

$$C_k = \left. \frac{\partial h(x_k)}{\partial x} \right|_{x=\hat{x}_k} = \begin{bmatrix} 1 & 0 & 0 & 0 & 0 \\ 0 & 1 & 0 & 0 & 0 \end{bmatrix} \quad (24)$$

3. Direct Torque Control

Direct Torque control (DTC) was proposed by I. Takahashi for controlling induction motors in the mid 1980s [6,7]. The main feature of DTC is to apply appropriate voltage space vectors for voltage source inverter (VSI) from a predefined switching table. Voltage vectors with their position in space is shown in Figure 1. The six voltage space-vectors ($V_1 - V_6$) divides the space domain into six equal-area sectors. Either V_0 or V_7 can be used to represent a null vector at the origin. As DTC does not rely on

pulse-width-modulation for generating the inverter voltage vectors, it requires less computational time with a reduced structure.

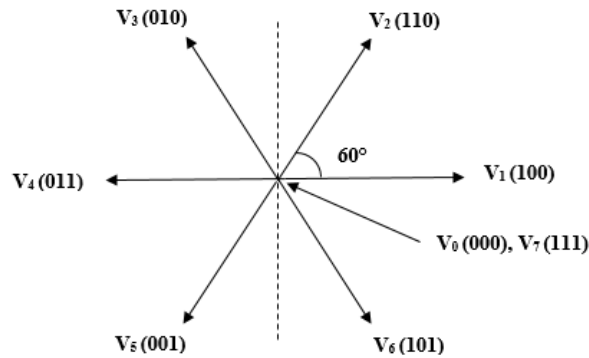


Figure 1. Voltage space vectors.

The overall scheme of the sensorless direct torque control with nonlinear Kalman filtering is shown in Figure 2. The desired stator flux λ_{ref} and torque τ_{ref} are compared with the estimated stator flux λ_{est} and torque τ_{est} in the hysteresis flux and torque controllers, respectively. The flux controller is a two-level hysteresis comparator, whereas the torque controller is a three-level hysteresis comparator. The flux and torque hysteresis comparators are illustrated in Figure 3.

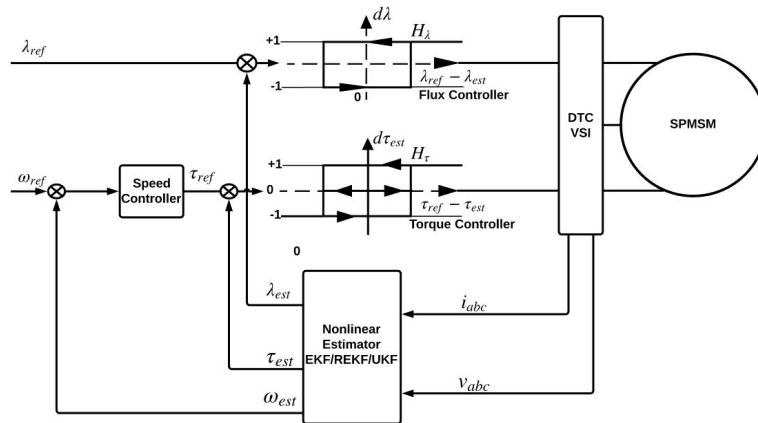


Figure 2. The proposed block diagram of DTC with nonlinear estimators.

The digitized output signal of the flux controller are defined based on

$$d\lambda = 1 \quad \text{for} \quad \lambda_{est} < \lambda_{ref} - H_\lambda \tag{25}$$

$$d\lambda = 0 \quad \text{for} \quad \lambda_{est} > \lambda_{ref} + H_\lambda, \tag{26}$$

where $2H_\lambda$ is the flux tolerance band.

The digitized output signal of the torque controller are defined based on

$$d\tau_{est} = 1 \quad \text{for} \quad \tau_{est} < H_\tau \tag{27}$$

$$d\tau_{est} = 0 \quad \text{for} \quad \tau_{est} = H_\tau \tag{28}$$

$$d\tau_{est} = -1 \quad \text{for} \quad \tau_{est} > H_\tau \tag{29}$$

where $2H_\tau$ is the torque tolerance band.

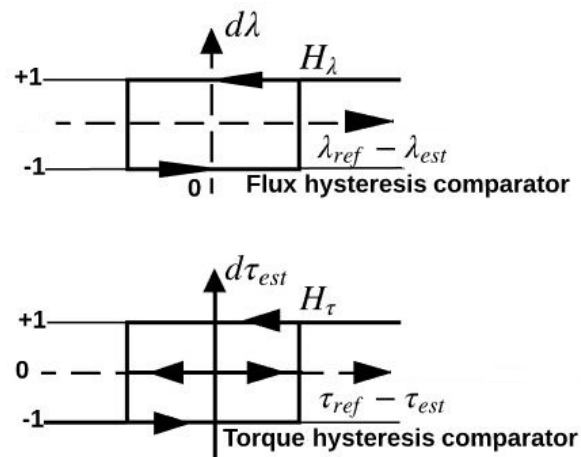


Figure 3. The flux and torque hysteresis comparators.

The stator flux sector index N is obtained from the computed angular position

$$\gamma_s = \tan^{-1} \frac{\lambda_\beta}{\lambda_\alpha} \quad (30)$$

Together with digitized variables $d\lambda$ and $d\tau_{est}$, a digital address for accessing an EPROM or EEPROM can be created. Hence, the appropriate voltage space-vector can be selected, which is governed by the switching rules in Table 1. Hence, the voltage source inverter can produce the desired three-phase voltages for controlling rotation.

Table 1. Direct Torque Control Switching Table.

$d\lambda$	$d\tau_{est}$	Number of Sectors (N)					
		1	2	3	4	5	6
$d\lambda = 1$	$d\tau_{est} = 1$	V_2	V_3	V_4	V_5	V_6	V_1
	$d\tau_{est} = 0$	V_7	V_0	V_7	V_0	V_7	V_0
	$d\tau_{est} = -1$	V_6	V_1	V_2	V_3	V_4	V_5
$d\lambda = 0$	$d\tau_{est} = 1$	V_3	V_4	V_5	V_6	V_1	V_2
	$d\tau_{est} = 0$	V_0	V_7	V_0	V_7	V_0	V_7
	$d\tau_{est} = -1$	V_5	V_6	V_1	V_2	V_3	V_4

4. Nonlinear Estimation

First, we revisit the traditional extended Kalman filter [28,29]. Over the past 40 years, EKF has been the most widely used nonlinear estimation technique for various industrial applications [30–32]. In order to provide a more reliable nonlinear estimation against external disturbances, noise, bad data and measurement failures, we propose the unscented Kalman filter (UKF) and the resilient extended Kalman filter (REKF)-based sensorless DTC technique for permanent magnet synchronous motors.

4.1. Extended Kalman Filter

Consider the discrete-time nonlinear system dynamics and measurement equation given as follows:

$$\begin{aligned}x_{k+1} &= f(x_k, u_k, v_k) \\ y_k &= h(x_k, u_k, w_k)\end{aligned}\quad (31)$$

The extended Kalman filter estimation consists two steps: time update and measurement update. First, define the following Jacobian matrices:

$$\begin{aligned}A_k &= \frac{\partial f}{\partial x} \Big|_{x=\hat{x}_k}, F_k = \frac{\partial f}{\partial v} \Big|_{x=\hat{x}_k} \\ C_k &= \frac{\partial h}{\partial x} \Big|_{x=\hat{x}_k}, G_k = \frac{\partial h}{\partial w} \Big|_{x=\hat{x}_k}\end{aligned}\quad (32)$$

For time update, we compute the priori covariance and priori state estimate

$$P_k^- = A_{k-1}P_{k-1}^+A_{k-1}^T + F_{k-1}V_{k-1}F_{k-1}^T \quad (33)$$

$$\hat{x}_k^- = f_{k-1}(\hat{x}_{k-1}^+, u_{k-1}, 0) \quad (34)$$

where V_k is the covariance matrix of process noise v_k at time step k . \hat{x}^- is the priori state estimate and P_k^- is the priori covariance matrix.

The measurement update can be summarized as follows

$$K_k = P_k^- C_k^T (C_k P_k^- C_k^T + G_k W_k G_k^T)^{-1} \quad (35)$$

$$\hat{x}_k^+ = \hat{x}_k^- + K_k [y_k - h_k(\hat{x}_k^-, 0)] \quad (36)$$

$$P_k^+ = (I - K_k C_k) P_k^- \quad (37)$$

where \hat{x}_k^+ is the posteriori state estimate; P_k^+ is the posteriori covariance matrix.

4.2. Resilient Extended Kalman Filter

Consider the discrete-time nonlinear stochastic system model and measurement equations as follows [33]:

$$\begin{aligned}x_{k+1} &= f(x_k) + v_k \\ y_k &= \begin{pmatrix} y_k^1 \\ y_k^2 \\ \vdots \\ y_k^p \end{pmatrix} = \begin{pmatrix} \gamma_k^1 h^1(x_k) + w_k^1 \\ \gamma_k^2 h^2(x_k) + w_k^2 \\ \vdots \\ \gamma_k^p h^p(x_k) + w_k^p \end{pmatrix},\end{aligned}\quad (38)$$

where

- $x_k \in \mathcal{R}^n$ state vector
- $v_k \in \mathcal{R}^n$ system noise
- $y_k \in \mathcal{R}^p$ measurement vector
- $w_k^i \in \mathcal{R}$ measurement noise in each phasor
- measurement unit and $w_k = [w_k^1, w_k^2, \dots, w_k^p]^T$
- f, h differentiable non-linear vector functions

The mean of initial state x_0 is $E[x_0] = \bar{x}_0$ and covariance of initial state x_0 is $X_0 = E[(x_0 - \bar{x}_0)(x_0 - \bar{x}_0)^T]$. The process and measurement noises, v_k and w_k , are white, zero mean, uncorrelated with each other and with x_0 , and have covariance V_k and W_k , respectively.

$$\begin{aligned} v_k &\sim (0, V_k), w_k \sim (0, W_k), \\ E[v_k v_j^T] &= V_k \delta_{k-j}, E[w_k w_j^T] = W_k \delta_{k-j}, \\ E[v_k w_j^T] &= 0, E[v_k x_0^T] = 0, E[w_k x_0^T] = 0 \end{aligned} \quad (39)$$

The scalar binary Bernoulli distributed random variables γ_k^i are with mean π_i and variance $\pi_i(1 - \pi_i)$ whose possible outcomes 0,1 are defined as $Prob(\gamma_k^i = 1) = \pi_i$ and $Prob(\gamma_k^i = 0) = 1 - \pi_i$. The formulation involves hard measurement failures, where the sensor either works properly or fails to provide reliable estimation.

By denoting

$$\Gamma_k = \text{diag}[\gamma_k^1, \gamma_k^2, \dots, \gamma_k^p] \quad (40)$$

$$h(x_k) = \text{diag}[h^1(x_k), h^2(x_k), \dots, h^p(x_k)] \quad (41)$$

the measurement equation can be written as

$$y_k = \Gamma_k h(x_k) + w_k \quad (42)$$

Our goal is to estimate the state vector x_k based on our knowledge of system dynamics and the availability of the noisy measurement y_k under the effect of sensor failures. The following discrete time nonlinear Luenberger observer is considered in this work.

$$\hat{x}_{k+1} = f(\hat{x}_k) + (K_k + \Delta_k)(y_k - \bar{\Gamma}_k h(\hat{x}_k)) \quad (43)$$

Although the filter gain should be K_k , due to computational or tuning uncertainties, it is erroneously implemented as $K_k + \Delta_k$. The term $\bar{\Gamma}_k$ is defined as

$$\bar{\Gamma}_k = E[\Gamma_k] = \text{diag}[\pi_1, \pi_2, \dots, \pi_p] \quad (44)$$

K_k is the feedback gain with additive uncertainty Δ_k . The uncertainty Δ_k , is assumed to have zero mean, bounded second moment and be uncorrelated with initial state, process and measurement noises, i.e.,

$$E[\Delta_k \Delta_k^T] \leq \delta I, E[\Delta_k^T x_0] = 0, E[\Delta_k^T v_k] = 0, E[\Delta_k w_k] = 0 \quad (45)$$

The resilient extended Kalman filter is defined as follows:

1. Initialization

$$\begin{aligned} \hat{x}_0 &= E[x_0] \\ P_0 &= E[(x_0 - \hat{x}_0)(x_0 - \hat{x}_0)^T] \end{aligned} \quad (46)$$

2. Computation of Jacobian matrices

$$A_k = \left. \frac{\partial f}{\partial x} \right|_{x=\hat{x}_k}, C_k = \left. \frac{\partial h}{\partial x} \right|_{x=\hat{x}_k} \quad (47)$$

3. For time steps $k = 1, 2, 3, \dots$, the estimator propagates by calculating the feedback gain

$$K_k^o = (A_k P_k C_k^T \bar{\Gamma}_k^T) [\bar{\Gamma}_k C_k P_k C_k^T \bar{\Gamma}_k^T + Y \otimes (h(\hat{x}_k) h^T(\hat{x}_k) + C_k P_k C_k^T) + W_k]^{-1} \tag{48}$$

from an upper bound on the local estimation error covariance

$$P_{k+1} = A_k P_k A_k^T + V_k + \lambda_{max} \{ \bar{\Gamma}_k C_k P_k C_k^T \bar{\Gamma}_k^T + W_k + Y \otimes (h(\hat{x}_k) h^T(\hat{x}_k) + C_k P_k C_k^T) \} \delta I - (A_k P_k C_k^T \bar{\Gamma}_k^T) [\bar{\Gamma}_k C_k P_k C_k^T \bar{\Gamma}_k^T + Y \otimes (h(\hat{x}_k) h^T(\hat{x}_k) + C_k P_k C_k^T) + W_k]^{-1} (\bar{\Gamma}_k C_k P_k A_k^T) \tag{49}$$

to be used in updating the state estimate as

$$\hat{x}_{k+1} = f(\hat{x}_k) + (K_k^o + \Delta_k)(y_k - \bar{\Gamma}_k h(\hat{x}_k)) \tag{50}$$

where

$$Y = \text{diag}[\pi_1(1 - \pi_1), \pi_2(1 - \pi_2), \dots, \pi_p(1 - \pi_p)] = \begin{pmatrix} \pi_1(1 - \pi_1) & 0 & \dots & 0 \\ 0 & \ddots & \ddots & \vdots \\ \vdots & \ddots & \ddots & 0 \\ 0 & \dots & 0 & \pi_p(1 - \pi_p) \end{pmatrix} \tag{51}$$

4.3. Unscented Kalman Filter

Consider the following system and measurement equations [34–38].

$$\begin{aligned} x_{k+1} &= f(x_k, u_k) + v_k \\ y_k &= h(x_k) + w_k, \end{aligned} \tag{52}$$

where

- $f(x_k, u_k)$ process model
- x_k state vectors
- u_k input state vectors
- $h(x_k)$ output model
- y_k output state vectors
- v_k process WGN
- w_k measurement WGN

The initial state x_o has a mean $\mu_o = E[x_o] = \bar{x}_o$ and a covariance $P_o = E[(x_o - \mu_o)(x_o - \mu_o)^T]$. The process and measurement noise are white Gaussian noise (WGN), which can be expressed as $v_k \sim (0, V_k)$, $w_k \sim (0, W_k)$. The initial state variables obey normal distribution with \bar{x}_o and P_o . The size of the sigma points is $x_\kappa = 2n + 1$, from which the UKF can be implemented using the following steps:

1. Initialization

$$\begin{aligned} \hat{x}_o &= E[x_o] \\ P_o &= E[(x_o - \bar{x}_o)(x_o - \bar{x}_o)^T] \end{aligned} \tag{53}$$

2. Define sigma points $\chi_k^{(s)}$ and weights ω^s for $s = 1, \dots, 2n$ as follows:

$$\chi_k^{(0)} = \hat{x}_k \quad (54)$$

$$\chi_k^{(s)} = \hat{x}_k + \tilde{x}_k^{(s)} \quad s = 1, \dots, 2n \quad (55)$$

$$\tilde{x}_k^{(s)} = (\sqrt{nP_k})_s^T \quad s = 1, \dots, n \quad (56)$$

$$\tilde{x}_k^{(n+s)} = -(\sqrt{nP_k})_s^T \quad s = 1, \dots, n \quad (57)$$

The weighing coefficients are determined by

$$\omega^s = \frac{1 - \omega^0}{2n} \quad s = 1, \dots, 2n \quad (58)$$

where the weight must agree

$$\sum_{s=0}^{2n} \omega^s = 1.$$

and $(\sqrt{nP_k})_s$ is s^{th} row or column of the matrix square root of nP_k .

3. Process Update

The priori mean and covariance of the estimated value \hat{x}_{k+1}^- can be obtained using the transformed sigma points as follows:

$$\hat{x}_{k+1} = \sum_{s=0}^{2n} \omega_s \cdot f(\chi_k^{(s)}, u_k) \quad (59)$$

$$P_{k+1}^- = \sum_{s=0}^{2n} \omega_s \cdot (f(\chi_k^{(s)}, u_k) - \hat{x}_{k+1}^-)(f(\chi_k^{(s)}, u_k) - \hat{x}_{k+1}^-)^T + V_k \quad (60)$$

4. Output Covariance Update

The predicted measurement is

$$\hat{y}_{k+1} = \sum_{s=0}^{2n} \omega_s \cdot h(\chi_k^{(s)}) \quad (61)$$

$$P_y = \sum_{s=0}^{2n} \omega_s \cdot (h(\chi_k^{(s)}) - \hat{y}_{k+1})(h(\chi_k^{(s)}) - \hat{y}_{k+1})^T + W_{k+1} \quad (62)$$

5. Cross-correlation Update

The cross-correlation P_{xy} is determined by

$$P_{xy} = \sum_{s=0}^{2n} \omega_s \cdot (f(\chi_k^{(s)}) - \hat{x}_{k+1})(h(\chi_k^{(s)}) - \hat{y}_{k+1})^T \quad (63)$$

6. Measurement Update

The final measurement update can be performed using normal Kalman filter equations as: The Kalman gain K_k can be written as follows:

$$K_{k+1} = P_{xy}P_y^{-1} \quad (64)$$

The posteriori covariance matrix P_{k+1} and the estimated state variable \hat{x}_{k+1} can be expressed as follows:

$$\hat{x}_{k+1} = \hat{x}_{k+1}^- + K_{k+1}(y_{k+1} - \hat{y}_{k+1}) \quad (65)$$

$$P_{k+1} = P_{k+1}^- - K_{k+1}P_y K_{k+1}^T \quad (66)$$

5. Computer Simulation Studies and Hardware Implementations

Computer simulation studies and Texas Instrument TMS320F28335 DSP processor implementations have been developed to show the efficiency of proposed sensorless direct torque control approach. The testing SPMSM parameters are summarized in Table 2. The hardware implementation is shown in Figure 4.

Table 2. The parameters of SPMSM.

Rated Power	400 W
Rated Torque	180 oz.in
Rated Voltage	220 V
Rated Current	2.7 A
Stator resistance, R_s	4.7 Ω
Stator inductance, L_s	13.3 mH
Rotor magnetic flux, λ_m	0.0785 Wb
Number of rotor poles, P	8
Moment of inertia, J	0.00439 oz.in.s ²

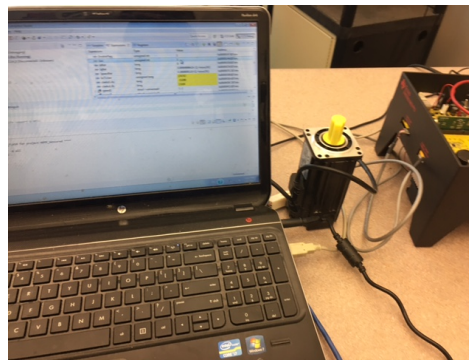
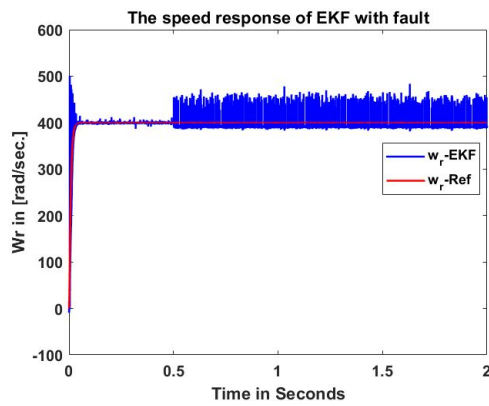


Figure 4. Hardware Implementation with TMS320F28335 DSP.

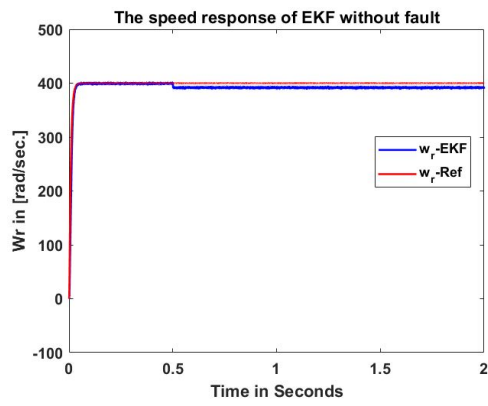
The final reference speed of SPMSM motor is set to be 400 mechanical rad/s. An external load of 1.5 Nm is applied at 0.5 s. Figures 5–8 show rotor speed, developed torque, stator flux, quadrature-axis stator current estimation comparisons, respectively. Figures in the first, second and third row show EKF, REKF and UKF estimation results, respectively. The first column figures are nonlinear estimation results under sensing failure condition. The second column figures are nonlinear estimation results without sensing failures. Note that EKF, UKF and REKF all converge to the real-state values. However, since the EKF uses first-order linearization to update the covariance of the state, it shows more estimation error compared with REKF and UKF.

Without measurement failures, the estimation error comparisons of EKF, UKF and REKF are summarized in Tables 3–5. In comparison with EKF and REKF, UKF shows superior accuracy in torque, speed, and current estimation, under the condition that all sensors work properly. Under no sensing failure condition, UKF tracks the real state variables more closely with less ripples, since it relies on

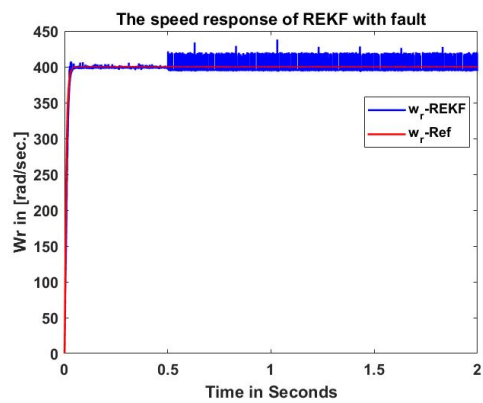
the unscented transformation to characterize the probability density function, without linearization involved. EKF truncates Taylor series of the mean at the first term, its prediction error of the mean value is in the second and higher order terms. EKF truncates at the first term of the covariance matrix, therefore, it is correct up to the second order with errors in fourth order term and above. UKF does not truncate any terms of the Taylor series, but uses sigma points through nonlinear transformation to decide the mean and covariance.



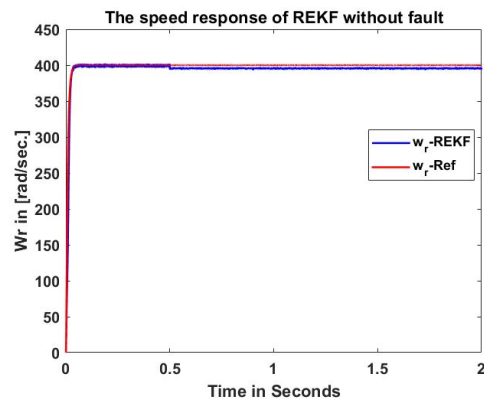
(a) The speed responses of EKF with fault



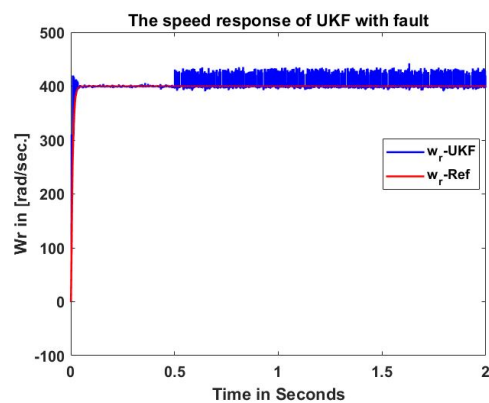
(d) The speed responses of EKF without fault



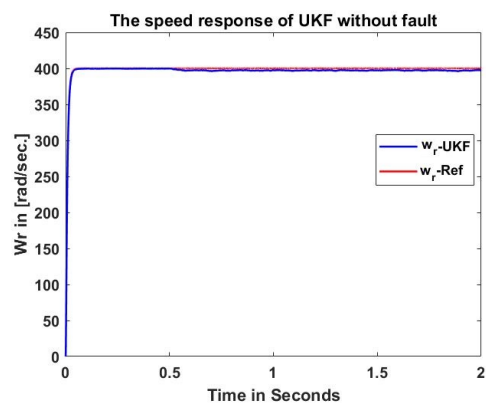
(b) The speed responses of REKF with fault



(e) The speed responses of REKF without fault



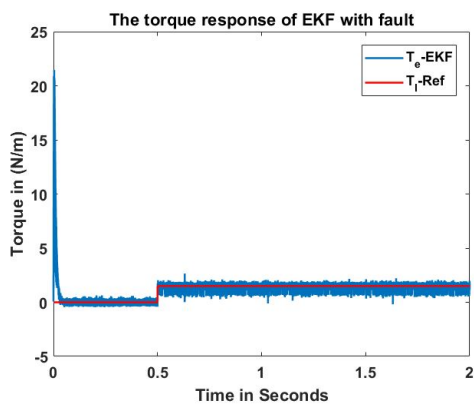
(c) The speed responses of UKF with fault



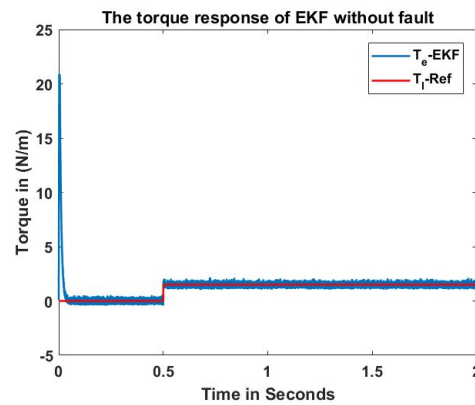
(f) The speed responses of UKF without fault

Figure 5. The speed comparison of DTC with EKF, REKF, and UKF.

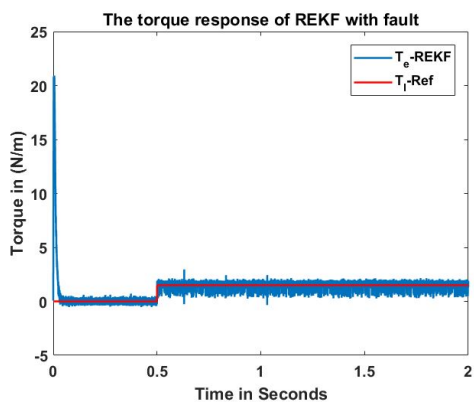
Under the sensing failure condition, computer simulations are conducted based on the assumption that each sensor has 5% failure rate. Scalar binary random variables following Bernoulli distribution are generated for the measurements in order to produce random sensing failures. In another word, the sensor either works properly or fail to provide true measurements with a probability of 5%. In this case, the resilient extended Kalman filter provides more reliable state estimation with greater accuracy compared to EKF and UKF, since the resilient extended Kalman filter is designed to handle measurement failures. Hence, REKF is a more robust nonlinear estimation approach.



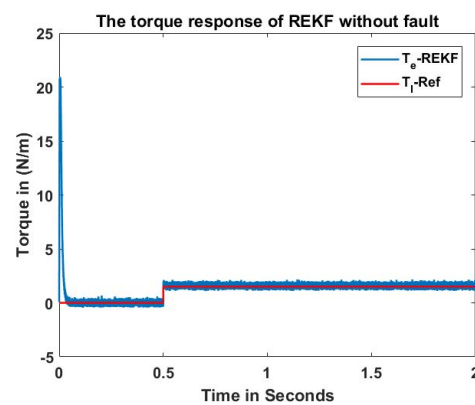
(a) The torque responses of EKF with fault



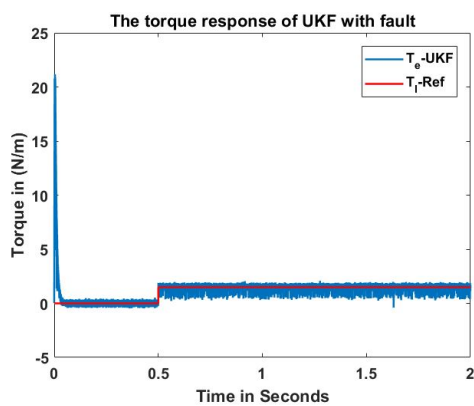
(d) The torque responses of EKF without fault



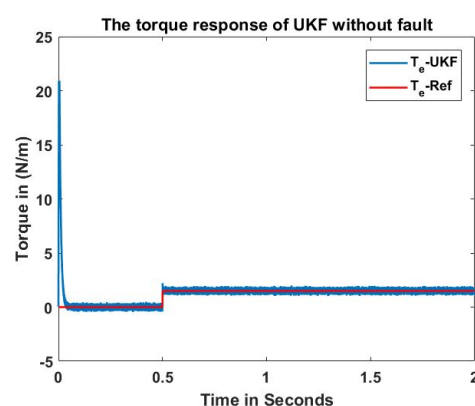
(b) The torque responses of REKF with fault



(e) The torque responses of REKF without fault

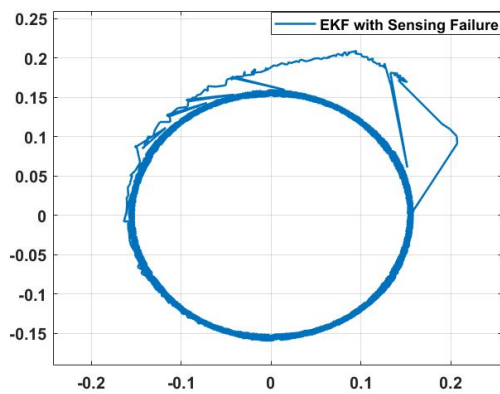


(c) The torque responses of UKF with fault

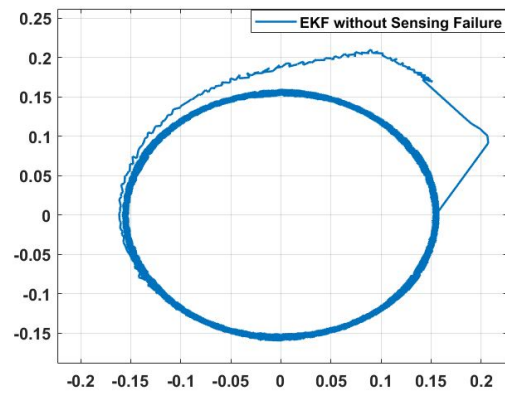


(f) The torque responses of UKF without fault

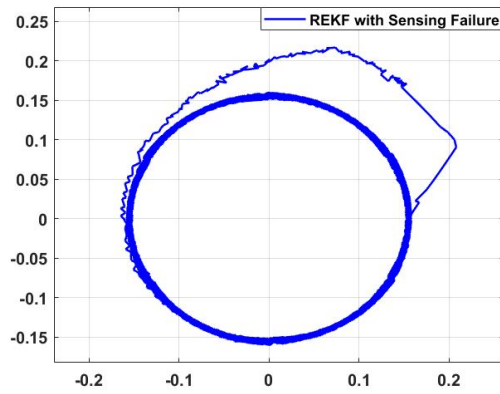
Figure 6. The torque comparison of DTC with EKF, REKF, and UKF.



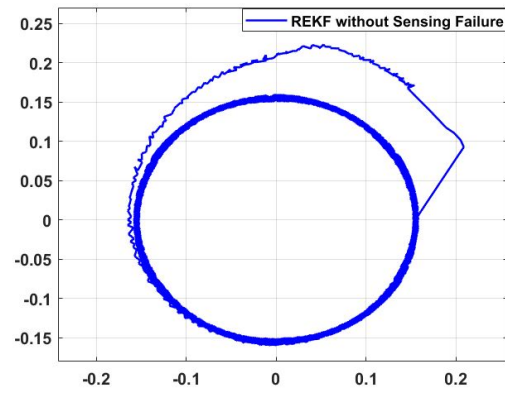
(a) The flux trajectory of EKF with fault



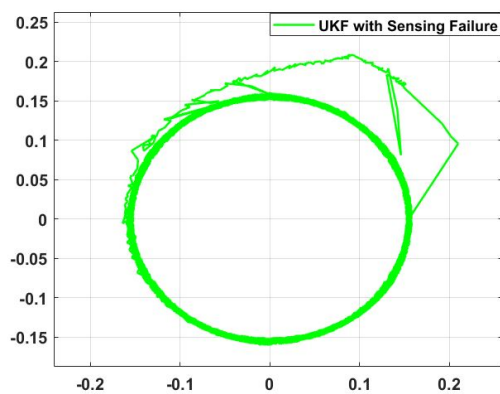
(d) The flux trajectory of EKF without fault



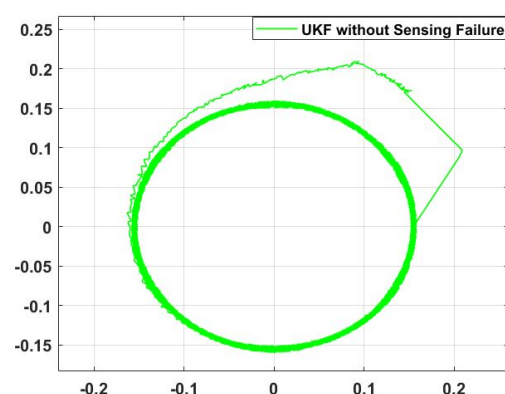
(b) The flux trajectory of REKF with fault



(e) The flux trajectory of REKF without fault



(c) The flux trajectory of UKF with fault



(f) The flux trajectory of UKF without fault

Figure 7. The stator flux trajectory comparison of DTC with EKF, REKF, and UKF.

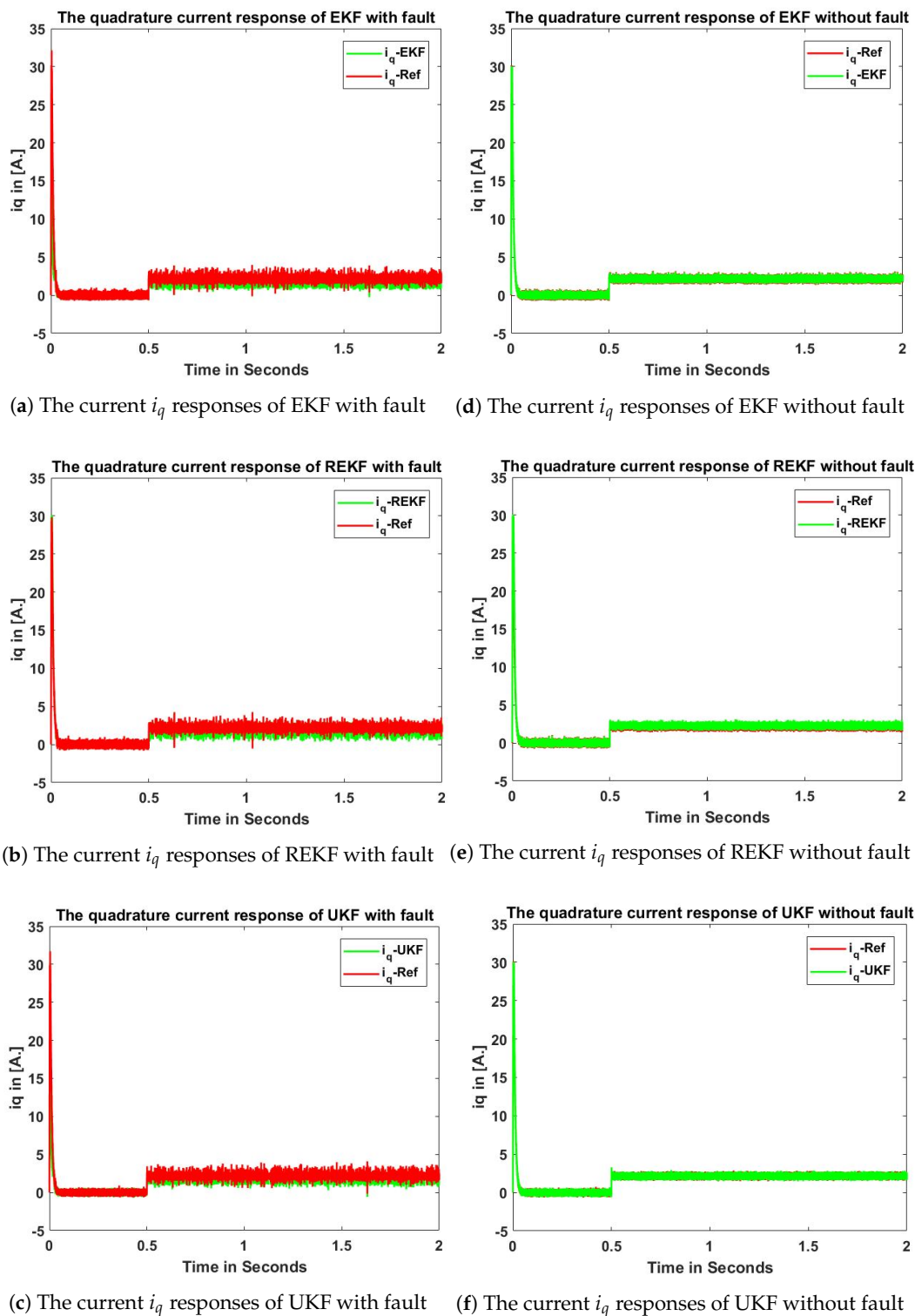


Figure 8. The current i_q comparison of DTC with EKF, REKF, and UKF.

Table 3. The torque estimation error comparison of EKF, REKF, and UKF without sensor failure.

Time Period (s)	EKF Estimation Error (N/m)	REKF Estimation Error (N/m)	UKF Estimation Error (N/m)
0 s–0.5 s	0.6089	0.6692	0.6675
0.5 s–1.0 s	0.2188	0.1987	0.1348
1.0 s–1.5 s	0.2180	0.1951	0.1653
1.5 s–2.0 s	0.2197	0.1938	0.1067

Table 4. The i_q estimation error comparison of EKF, REKF, and UKF without sensor failure.

Time Period (s)	EKF Estimation Error (A)	REKF Estimation Error (A)	UKF Estimation Error (A)
0 s–0.5 s	22.3889	22.4353	13.775
0.5 s–1.0 s	0.3985	0.3629	0.1491
1.0 s–1.5 s	0.3917	0.3718	0.2004
1.5 s–2.0 s	0.3971	0.3619	0.1842

Table 5. The speed estimation error comparison of EKF, REKF, and UKF without sensor failure.

Time Period (s)	EKF Estimation Error (rad/s)	REKF Estimation Error (rad/s)	UKF Estimation Error (rad/s)
0 s–0.5 s	10.7434	11.2876	1.7615
0.5 s–1.0 s	4.3493	3.0354	0.5825
1.0 s–1.5 s	4.3622	2.9833	0.7320
1.5 s–2.0 s	4.3790	3.0036	0.7345

6. Conclusions

Direct torque control combines the benefits of direct flux and torque control into an adjustable speed drive, which does not require pulse-width-modulation or coordinate transforms. The paper presented a comparative study of sensorless direct torque control approaches of surface-mounted permanent magnet synchronous motors with the unscented Kalman filter (UKF), the resilient extended Kalman filter (REKF), and the extended Kalman filter (EKF). As demonstrated by simulation and implementation results, EKF, REKF, and UKF all track the state variables effectively. However, REKF is a preferred estimation method when sensors randomly fail to provide accurate measurements; whereas UKF is a superior method in state variables estimation when all sensors provide accurate measurements.

Author Contributions: All authors contributed equally in the presented research, and all authors approved the final manuscript.

Conflicts of Interest: The authors declare no conflicts of interest.

Nomenclature

i_a, i_b, i_c and v_a, v_b, v_c	3-phase currents and voltages
R_s, L_s, i_s, v_s	stator resistance, inductance, current and voltage
v_d, v_q	direct and quadrature axis voltages
i_d, i_q	direct and quadrature axis currents
λ_s, λ_m	stator and rotor magnetic flux linkages
λ_d, λ_q	direct and quadrature axis flux linkages
$\lambda_\alpha, \lambda_\beta$	α and β axis flux linkages
L_d, L_q	direct and quadrature axis inductances
ω_e, ω_m	electrical and mechanical angular speed
P, J, D	number of pole, moment of inertia, and viscous friction coefficient

θ_e	electrical angular position
$\tau_e, \tau_l, \tau_{est}, \tau_{ref}$	electrical, load, estimated, and reference torques
γ_s	computed angular position
$d\lambda_{est}, d\tau_{est}$	digitized variables for flux and torque controller
H_λ, H_τ	flux and torque tolerance bands
P_k^-, x_k^-	priori covariance and priori state estimate
P_{k+1}	posteriori covariance matrix
\hat{x}_{k+1}	estimated state variable
K_k	Kalman gain
v_k, w_k	process and measurement noise
V_k, W_k	covariance matrix of process and measurement noise v, w at the k^{th} time step
γ_k^i	scalar binary random variables following the Bernoulli-distribution
Δ_k	additive uncertainty in Kalman gain
P_{xy}	cross-correlation matrix
$\chi_k^{(s)}$	sigma points
ω^s	weighing coefficients

References

- Xu, Z.; Rahman, M.F. Direct Torque and Flux Regulation of an IPM Synchronous Motor Drive Using Variable Structure Control Approach. *IEEE Trans. Power Electron.* **2007**, *22*, 2487–2498.
- Cunha, J.P.V.S.; Costa, R.R.; Lizarralde, F.; Hsu, L. Peaking free variable structure control of uncertain linear systems based on a high-gain observer. *Automatica* **2009**, *45*, 1156–1164. [[CrossRef](#)]
- Paicu, M.C.; Boldea, I.; Andreescu, G.D.; Blaabjerg, F. Very low speed performance of active flux based sensorless control: interior permanent magnet synchronous motor vector control versus direct torque and flux control. *IET Electr. Power Appl.* **2009**, *3*, 551–561. [[CrossRef](#)]
- Boazzo, B.; Pellegrino, G. Model-Based Direct Flux Vector Control of Permanent-Magnet Synchronous Motor Drives. *IEEE Trans. Ind. Appl.* **2015**, *51*, 3126–3136. [[CrossRef](#)]
- Drobic, K.; Nemeč, M.; Nedeljkovic, D.; Ambrozic, V. Predictive Direct Control Applied to AC Drives and Active Power Filter. *IEEE Trans. Ind. Electron.* **2009**, *56*, 1884–1893. [[CrossRef](#)]
- Noguchi, T.; Takahashi, I. Quick torque response control of an induction motor based on a new concept. *IEEJ Tech. Meeting Rotating Mach* **1984**, *1*, 61–70.
- Takahashi, I.; Noguchi, T. A new quick-response and high-efficiency control strategy of an induction motor. *IEEE Trans. Ind. Appl.* **1986**, *IA-22*, 820–827. [[CrossRef](#)]
- Rahman, M.F.; Zhong, L.; Haque, M.E.; Rahman, M.A. A direct torque-controlled interior permanent-magnet synchronous motor drive without a speed sensor. *IEEE Trans. Energy Conver.* **2003**, *18*, 17–22. [[CrossRef](#)]
- Haque, M.E.; Rahman, M.F. Incorporating control trajectories with the direct torque control scheme of interior permanent magnet synchronous motor drive. *IET Electr. Power Appl.* **2009**, *3*, 93–101. [[CrossRef](#)]
- Boldea, I.; Paicu, M.C.; Andreescu, G.D.; Blaabjerg, F. Active Flux DTFC-SVM Sensorless Control of IPMSM. *IEEE Trans. Energy Conver.* **2009**, *24*, 314–322. [[CrossRef](#)]
- Faiz, J.; Mohseni-Zonoozi, S.H. A novel technique for estimation and control of stator flux of a salient-pole PMSM in DTC method based on MTPF. *IEEE Trans. Ind. Electron.* **2003**, *50*, 262–271. [[CrossRef](#)]
- Buja, G.S.; Kazmierkowski, M.P. Direct torque control of PWM inverter-fed AC motors—A survey. *IEEE Trans. Ind. Electron.* **2004**, *51*, 744–757. [[CrossRef](#)]
- Mohamed, Y.A.R.I. A Newly Designed Instantaneous-Torque Control of Direct-Drive PMSM Servo Actuator With Improved Torque Estimation and Control Characteristics. *IEEE Trans. Ind. Electron.* **2007**, *54*, 2864–2873. [[CrossRef](#)]
- Mohamed, Y.A.R.I. Direct Instantaneous Torque Control in Direct Drive Permanent Magnet Synchronous Motors: a New Approach. *IEEE Trans. Energy Conver.* **2007**, *22*, 829–838. [[CrossRef](#)]
- Boldea, I.; Agarlita, S.C. The active flux concept for motion-sensorless unified AC drives: A review. In Proceedings of the 2011 International Aegean Conference on Electrical Machines and Power Electronics and 2011 Electromotion Joint Conference (ACEMP), Istanbul, Turkey, 8–10 September 2011; pp. 1–16.

16. Vyncke, T.J.; Boel, R.K.; Melkebeek, J.A.A. A comparison of stator flux linkage estimators for a direct torque controlled PMSM drive. In Proceedings of the 35th Annual Conference of IEEE Industrial Electronics (IECON '09), Porto, Portugal, 3–5 November 2009; pp. 971–978.
17. Inoue, Y.; Morimoto, S.; Sanada, M. Control Method Suitable for Direct-Torque-Control-Based Motor Drive System Satisfying Voltage and Current Limitations. *IEEE Trans. Ind. Appl.* **2012**, *48*, 970–976. [[CrossRef](#)]
18. Xu, Z.; Rahman, M.F. Comparison of a Sliding Observer and a Kalman Filter for Direct-Torque-Controlled IPM Synchronous Motor Drives. *IEEE Trans. Ind. Electron.* **2012**, *59*, 4179–4188. [[CrossRef](#)]
19. Mercorelli, P. A Two-Stage Sliding-Mode High-Gain Observer to Reduce Uncertainties and Disturbances Effects for Sensorless Control in Automotive Applications. *IEEE Trans. Ind. Electron.* **2015**, *62*, 5929–5940. [[CrossRef](#)]
20. Bernardes, T.; Montagner, V.F.; Gründling, H.A.; Pinheiro, H. Discrete-Time Sliding Mode Observer for Sensorless Vector Control of Permanent Magnet Synchronous Machine. *IEEE Trans. Ind. Electron.* **2014**, *61*, 1679–1691. [[CrossRef](#)]
21. Xu, Z.; Rahman, M.F. An extended Kalman filter observer for the direct torque controlled interior permanent magnet synchronous motor drive. In Proceedings of the Fifth International Conference on Power Electronics and Drive Systems, Singapore, 17–20 November 2003; pp. 686–691.
22. Xu, Z.; Rahman, M.F. Sensorless sliding mode control of an interior permanent magnet synchronous motor based on extended Kalman filter. In Proceedings of the Fifth International Conference on Power Electronics and Drive Systems, Singapore, 17–20 November 2003; pp. 722–727.
23. Foo, G.; Sayeef, S.; Rahman, M.F. SVM direct torque controlled interior permanent magnet synchronous motor drive using an extended Kalman Filter. In Proceedings of the 4th IET Conference on Power Electronics, Machines and Drives, York, UK, 2–4 April 2008; pp. 712–716.
24. Vyncke, T.J.; Boel, R.K.; Melkebeek, J.A.A. On Extended Kalman Filters with augmented state vectors for the stator flux estimation in SPMSMs. In Proceedings of the 2010 Twenty-Fifth Annual IEEE Applied Power Electronics Conference and Exposition (APEC), Palm Springs, CA, USA, 21–25 February 2010; pp. 1711–1718.
25. Mercorelli, P. A Hysteresis Hybrid Extended Kalman Filter as an Observer for Sensorless Valve Control in Camless Internal Combustion Engines. *IEEE Trans. Ind. Appl.* **2012**, *48*, 1940–1949. [[CrossRef](#)]
26. Mercorelli, P. A Two-Stage Augmented Extended Kalman Filter as an Observer for Sensorless Valve Control in Camless Internal Combustion Engines. *IEEE Trans. Ind. Electron.* **2012**, *59*, 4236–4247. [[CrossRef](#)]
27. Vyncke, T.J.; Boel, R.K.; Melkebeek, J.A.A. On the stator flux linkage estimation of an PMSM with Extended Kalman Filters. In Proceedings of the 5th IET International Conference on Power Electronics, Machines and Drives (PEMD 2010), Brighton, UK, 19–21 April 2010; pp. 1–6.
28. Reif, K.; Gunther, S.; Yaz, E.; Unbehauen, R. Stochastic stability of the discrete-time extended Kalman filter. *IEEE Trans. Autom. Control* **1999**, *44*, 714–728. [[CrossRef](#)]
29. Reif, K.; Gunther, S.; Yaz, E.; Unbehauen, R. Stochastic stability of the continuous-time extended Kalman filter. *IEE Proc. Control Theory Appl.* **2000**, *147*, 45–52. [[CrossRef](#)]
30. Haus, B.; Aschemann, H.; Mercorelli, P. Tracking Control of a Piezo-Hydraulic Actuator Using Input-Output Linearization and a Cascaded Extended Kalman Filter Structure. *J. Franklin Inst.* **2017**, doi:10.1016/j.jfranklin.2017.07.042. [[CrossRef](#)]
31. Mercorelli, P. An adaptive and optimized switching observer for sensorless control of an electromagnetic valve actuator in camless internal combustion engines *Asian J. Control* **2014**, *16*, 959–973.
32. Chen, L.; Mercorelli, P.; Liu, S. A Kalman estimator for detecting repetitive disturbances. In Proceedings of the 2005 American Control Conference, Portland, OR, USA, 8–10 June 2005; Volume 3, pp. 1631–1636.
33. Wang, X.; Yaz, E.E. Stochastically resilient extended Kalman filtering for discrete-time nonlinear systems with sensor failures. *Int. J. Syst. Sci.* **2014**, *45*, doi:10.1080/00207721.2013.879257. [[CrossRef](#)]
34. Wan, E.A.; Van Der Merwe, R. The unscented Kalman filter for nonlinear estimation. In Proceedings of the Adaptive Systems for Signal Processing, Communications, and Control Symposium 2000 (AS-SPCC), Lake Louise, AB, Canada, 4 October 2000; pp. 153–158.
35. Wan, E.A.; Van Der Merwe, R. *The Unscented Kalman Filter, Kalman Filtering and Neural Networks*; John Wiley & Sons, Inc.: Hoboken, NJ, USA, 2002.
36. Julier, S.; Uhlmann, J. A New extension of the Kalman filter to Nonlinear Systems. In *Proceedings Volume 3068, Signal Processing, Sensor Fusion, and Target Recognition VI*; International Symposium Aerospace/Defense Sensing, Simulation and Controls, SPIE: Orlando, FL, USA, 1997; pp. 182–193.

37. Julier, S.; Uhlmann, J.K.; Durrant-Whyte, H.F. A new approach for filtering nonlinear systems. In Proceedings of the 1995 American Control Conference, Seattle, WA, USA, 21–23 June 1995; Volume 3, pp. 1628–1632.
38. Simon, D. *Optimal State Estimation: Kalman, H-Infinity, and Nonlinear Approaches*, 1st ed.; Wiley & Sons, Inc.: Hoboken, NJ, USA, 2006.



© 2018 by the authors. Licensee MDPI, Basel, Switzerland. This article is an open access article distributed under the terms and conditions of the Creative Commons Attribution (CC BY) license (<http://creativecommons.org/licenses/by/4.0/>).